Supplemental Material of "Yang monopoles and emergent three-dimensional topological defects in interacting bosons"

Yangqian Yan, Qi Zhou
Department of Physics and Astronomy, Purdue University, West Lafayette, IN, 47906
(Dated: March 14, 2018)

DEFINITION OF C_2

The non-abelian Berry connection A_ν^{mn}, non-abelian Berry curvature $F_{\mu\nu}^{mn}$, and non-abelian second Chern number are defined as [1].

$$A_\nu^{mn} = -i\langle\Psi_m|\partial_\mu|\Psi_n\rangle, \quad F_{\mu\nu}^{mn} = \partial_\mu A_\nu^{mn} - \partial_\nu A_\mu^{mn} + i[A_\mu, A_\nu]^{mn} \tag{S1}$$

$$C_2 = \frac{1}{32\pi^2}\int_{S^4} d\mathbf{R}\epsilon_{\mu\nu\rho\lambda}(\mathrm{Tr}[F_{\mu\nu}F_{\rho\lambda}] - \mathrm{Tr}[F_{\mu\nu}]\mathrm{Tr}[F_{\rho\lambda}]). \tag{S2}$$

NON-INTERACTING C_2

Single-particle ground state of the Hamiltonian in Eq. (1) of the main text is doubly degenerate. Denote the two states as ψ_a and ψ_b, and define $A_{\mu\nu}^{mn} = -i\langle\partial_\mu\psi_m|\partial_\nu\psi_n\rangle$, the Berry curvature reads

$$F_{\mu\nu}^{mn} = A_{\mu\nu}^{mn} - A_{\nu\mu}^{mn} + i[A_\mu, A_\nu]. \tag{S3}$$

Because of the time-reversal symmetry, the traces of the Berry connection and the Berry curvature are zero,

$$A_\mu^{aa} = -A_\mu^{bb}, \quad \mathrm{Tr}F_{\mu\nu} = 0. \tag{S4}$$

We also have $A_{\mu\nu}^{aa} = A_{\nu\mu}^{bb}$. Defining

$$\tilde{A}_{\mu\nu} = \begin{pmatrix} A_{\mu\nu}^{aa} & A_{\mu\nu}^{ab} \\ A_{\mu\nu}^{ba} & -A_{\mu\nu}^{aa} \end{pmatrix} \tag{S5}$$

$$\tilde{F}_{\mu\nu} = \tilde{A}_{\mu\nu} + iA_\mu A_\nu, \tag{S6}$$

and using the property of the Levi-Civita symbol, we express the second Chern number using an alternative form,

$$C_2^o(1) = \frac{1}{32\pi^2}\int_{S^4} d\mathbf{R}\epsilon_{\mu\nu\rho\lambda}\mathrm{Tr}[F_{\mu\nu}F_{\rho\lambda}] = \frac{1}{8\pi^2}\int_{S^4} d\mathbf{R}\epsilon_{\mu\nu\rho\lambda}\mathrm{Tr}[\tilde{F}_{\mu\nu}\tilde{F}_{\rho\lambda}]. \tag{S7}$$

The above results can be generalized to N particles.

For N non-interacting bosons, there are $N+1$ degenerate ground states. Using Fock states as basis states, the ground state reads $|N-i, i\rangle$, where i takes the values of $0, 1, 2, \ldots, N$; here $|N-i, i\rangle$ represent the $N-i$ bosons in state ψ_a and i bosons in state ψ_b. The Berry connection A_μ and matrix $A_{\mu\nu}$ are tridiagonal in the Fock state basis.

$$A_\mu^{i-1,i} = -i\langle N-i+1, i-1|\partial_\mu|N-i, i\rangle = \sqrt{i(N-1+1)}A_\mu^{ab} \tag{S8}$$

$$A_\mu^{i,i-1} = -i\langle N-i, i|\partial_\mu|N-i+1, i-1\rangle = \sqrt{i(N-1+1)}A_\mu^{ba} \tag{S9}$$

$$A_\mu^{i,i} = -i\langle N-i, i|\partial_\mu|N-i, i\rangle = (N-i)A_\mu^{aa} + iA_\mu^{bb} = (N-2i)A_\mu^{aa}. \tag{S10}$$

The same holds for the $\tilde{A}_{\mu\nu}$ matrix,

$$\tilde{A}_{\mu\nu}^{i-1,i} = -i\langle N-i+1, i-1|\overleftarrow{\partial_\mu}\overrightarrow{\partial_\nu}|N-i, i\rangle = \sqrt{i(N-1+1)}A_{\mu\nu}^{ab} \tag{S11}$$

$$\tilde{A}_{\mu\nu}^{i,i-1} = -i\langle N-i, i|\overleftarrow{\partial_\mu}\overrightarrow{\partial_\nu}|N-i+1, i-1\rangle = \sqrt{i(N-1+1)}A_{\mu\nu}^{ba} \tag{S12}$$

$$\tilde{A}_{\mu\nu}^{i,i} = (N-2i)A_{\mu\nu}^{aa}. \tag{S13}$$

Note that A_{μ}^{xy} and $A_{\mu\nu}^{xy}$ are for single particle if x, y is a or b and are for N particles elsewise. Same as that for $N = 1$, the second Chern number for arbitrary N can also be calculated using Eq. (S5).

We break the integrand $\epsilon_{\mu\nu\rho\lambda}\mathrm{Tr}[\tilde{F}_{\mu\nu}\tilde{F}_{\rho\lambda}]$ into two parts, $\epsilon_{\mu\nu\rho\lambda}\mathrm{Tr}[\tilde{F}_{\mu\nu}\tilde{A}_{\rho\lambda}]$ and $2i\epsilon_{\mu\nu\rho\lambda}\mathrm{Tr}[\tilde{A}_{\mu\nu}A_{\rho}A_{\lambda}]$ (note that $\epsilon_{\mu\nu\rho\lambda}\mathrm{Tr}[A_{\mu}A_{\nu}A_{\rho}A_{\lambda}]$ is 0). Writing down the trace explicitly and expressing the two terms in terms of the single particle quantities, we obtain

$$\mathrm{Tr}[\tilde{A}_{\mu\nu}\tilde{A}_{\rho\lambda}] = \sum_i \tilde{A}_{\mu\nu}^{ii}\tilde{A}_{\rho\lambda}^{ii} + \sum_i \tilde{A}_{\mu\nu}^{i,i+1}\tilde{A}_{\rho\lambda}^{i+1,i} + \sum_i \tilde{A}_{\mu\nu}^{i,i-1}\tilde{A}_{\rho\lambda}^{i-1,i} \tag{S14}$$

$$= \sum_{i=0}^{N}(N-2i)^2\tilde{A}_{\mu\nu}^{aa}\tilde{A}_{\rho\lambda}^{aa} + \sum_{i=0}^{N-1}(i+1)(N-i)\left(\tilde{A}_{\mu\nu}^{ab}\tilde{A}_{\rho\lambda}^{ba} + \tilde{A}_{\mu\nu}^{ba}\tilde{A}_{\rho\lambda}^{ab}\right) \tag{S15}$$

$$\mathrm{Tr}[\tilde{A}_{\mu\nu}A_{\rho}A_{\lambda}] = \sum_i \tilde{A}_{\mu\nu}^{ii}\left(A_{\rho}^{i,i+1}A_{\lambda}^{i+1,i} + A_{\rho}^{i,i-1}A_{\lambda}^{i-1,i}\right) \tag{S16}$$

$$+ \sum_i \tilde{A}_{\mu\nu}^{i,i-1}\left(A_{\rho}^{i-1,i-1}A_{\lambda}^{i-1,i} + A_{\rho}^{i-1,i}A_{\lambda}^{i,i}\right) \tag{S17}$$

$$+ \sum_i \tilde{A}_{\mu\nu}^{i,i+1}\left(A_{\rho}^{i+1,i+1}A_{\lambda}^{i+1,i} + A_{\rho}^{i+1,i}A_{\lambda}^{i,i}\right) \tag{S18}$$

$$= \sum_{i=0}^{N}(N-2i)(N-i)(i+1)\left(A_{\mu\nu}^{aa}A_{\rho}^{ab}A_{\lambda}^{ba} + A_{\mu\nu}^{ba}A_{\rho}^{aa}A_{\lambda}^{ab} + A_{\mu\nu}^{ab}A_{\rho}^{ba}A_{\lambda}^{aa}\right) \tag{S19}$$

$$+ \sum_{i=0}^{N}(N-2i)(N-i+1)i\left(A_{\mu\nu}^{aa}A_{\rho}^{ba}A_{\lambda}^{ab} + A_{\mu\nu}^{ba}A_{\rho}^{ab}A_{\lambda}^{aa} + A_{\mu\nu}^{ab}A_{\rho}^{aa}A_{\lambda}^{ba}\right) \tag{S20}$$

Using the identity

$$\frac{1}{6}N(N+1)(N+2) = -\sum_{i=0}^{N}(N-2i)(N-i+1)i, \tag{S21}$$

we write $C_2^0(N)$ using $C_2^0(1)$,

$$C_2^0(N) = \frac{1}{6}N(N+1)(N+2)C_2^0(1) = \frac{1}{6}N(N+1)(N+2). \tag{S22}$$

LOCATION AND CHARGE OF YANG MONOPOLES FOR ODD N AND POSITIVE g

Along the R_5 axis, all off-diagonal couplings disappear and Fock states become the eigenstates. Varying R_5, we find N possible points on this axis where there exist four-fold degeneracy.

(a) $N = 4m + 1$ for integer m

The four states, $|m-l+1, m+l, m+l, m-l\rangle, |m-l, m+l+1, m+l, m-l\rangle$, $|m-l, m+l, m+l+1, m-l\rangle$, and $|m-l, m+l, m+l, m-l+1\rangle$ are degenerate when $R_5 = -2lg$, where $l = -m, -m+1, \ldots, m-1, m$. The effective Hamiltonian reads

$$\tilde{\epsilon}_i = \epsilon_i \tag{S23}$$

$$\tilde{t}_{ij} = t_{ij}\sqrt{(m-l+1)(m+l+1)}. \tag{S24}$$

The extra Bose enhancement factor comparing to the single particle Hamiltonian does not change the second Chern number, so $C_2 = 1$.

At $R_5 = -(2l+1)g$, the other four states, $|m-l-1, m+l+1, m+l+1, m-l\rangle, |m-l, m+l, m+l+1, m-l\rangle$, $|m-l, m+l+1, m+l, m-l\rangle$, and $|m-l-1, m+l+1, m+l+1, m-l\rangle$ are degenerate, where $l = -m, -m+$

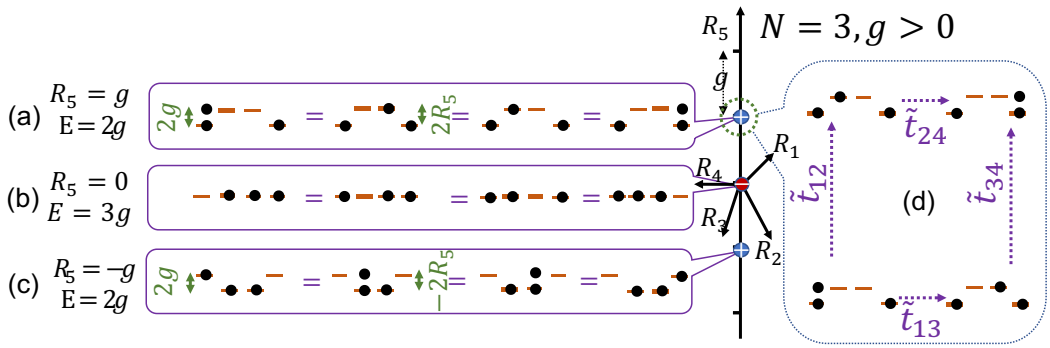

FIG. S1. (Color online) Schematic of Yang monopoles for 3 particles with positive interaction strength g. Blue (red) spheres show the positively (negatively) charged monopoles. Charges are denoted inside the sphere. The insects (a), (b), and (c) show the degenerate states at $R_5 = g, 0,$, and $-g$,respectively; here $R_1 = R_2 = R_3 = R_4 = 0$. The insect (d) shows the effective Hamiltonian in the vicinity of $R_5 = g, R_1 = R_2 = R_3 = R_4 = 0$. Orange solid lines and black dots represent single particle states and bosons, respectively. Purple dotted arrows show effective couplings.

$1, \ldots, m-2, m-1$. The effective Hamiltonian reads

$$\tilde{\epsilon}_i = -\epsilon_i \tag{S25}$$

$$\tilde{t}_{ij} = t_{ij}^* \sqrt{(m-l)(m+l+1)}. \tag{S26}$$

The extra Bose enhancement factor together with an additional phase factor $e^{i\pi}$ comparing to the single particle Hamiltonian does not change the second Chern number but flipping the sign of the diagonal terms changes C_2 to -1.

(b) $N = 4m+3$ for integer m

At $R_5 = -2lg$, the four states, $|m-l, m+l+1, m+l+1, m-l+1\rangle$, $|m-l+1, m+l, m+l+1, m-l+1\rangle$, $|m-1, m+l+1, m+l, m-l+1\rangle$, and $|m-l+1, m+l+1, m+l+1, m-l\rangle$ are degenerate, where $l = -m, -m+1, \ldots, m-1, m$. The effective Hamiltonian reads

$$\tilde{\epsilon}_i = -\epsilon_i \tag{S27}$$

$$\tilde{t}_{ij} = t_{ij}^* \sqrt{(m-l+1)(m+l+1)}. \tag{S28}$$

Similar to case (a), $C_2 = -1$.

At $R_5 = -(2l+1)g$, the four states, $|m-l+1, m+l+1, m+l+1, m-l\rangle$, $|m-l, m+l+2, m+l+1, m-l\rangle$, $|m-l, m+l+1, m+l+2, m-l\rangle$, and $|m-l, m+l+1, m+l+1, m-l+1\rangle$ are degenerate, where $l = -m-1, -m, \ldots, m-1, m$. The effective Hamiltonian reads

$$\tilde{\epsilon}_i = \epsilon_i \tag{S29}$$

$$\tilde{t}_{ij} = t_{ij} \sqrt{(m-l+1)(m+l+2)}. \tag{S30}$$

Similar to case (a), $C_2 = 1$.

For example, Fig. S1(d) illustrates the effective Hamiltonian for $N = 3$ and $R_5 = g$. The onsite energy different balances off the repulsive energy for the sites with two particles. Thus, all the four states has the same energy and as the coupling R_1, R_2, R_3, R_4 approaches zero, the four states becomes the eigenstates and four-fold degeneracy emerges.

EXPRESSION FOR c_N

At the origin, $|N,0,0,0\rangle$, $|0,N,0,0\rangle$, $|0,0,N,0\rangle$, $|0,0,0,N\rangle$ are the four degenerate many-body ground states. Treating the $|R|$ as a small parameter, the lowest order coupling reads

$$\langle N,0,0,0|\hat{H}_{\text{eff}}|0,N,0,0\rangle = \frac{\prod_{i=0}^{N-1} \langle N-i,i,0,0|\hat{K}|N-i-1,i+1,0,0\rangle}{\prod_{i=1}^{N-1} \left(\langle N-i,i,0,0|\hat{U}|N-i,i,0,0\rangle - \langle N,0,0,0|\hat{U}|N,0,0,0\rangle\right)}. \tag{S31}$$

Other terms can be written similarly. Comparing with the expression in the main text, we have

$$c_N = \frac{\prod_{i=0}^{N-1}\sqrt{(N-i)(i+1)}}{\prod_{i=1}^{N-1}\left[(N-i)^2+i^2-N^2\right]}. \tag{S32}$$

TOPOLOGICAL INVARIANTS

The Wilson line $W_{ij}(\phi)$ is defined by $W_{ij}(\phi) = \langle\Psi_i(\pi,\phi)|\hat{W}|\Psi_j(0,\phi)\rangle$, where $|\Psi_{i=1,2}(0,\phi)\rangle$ and $|\Psi_{i=1,2}(\pi,\phi)\rangle$ are the lowest two eigenstate states at the north and south poles, respectively, $\phi \in [0, 2\pi)$ is the azimuthal angle, and $\hat{W} = \prod_{k=1}^{\mathcal{N}} \hat{P}_k$, $\hat{P}_k = \sum_{i=1}^{2} |\Psi_i(\theta_k,\phi)\rangle\langle\Psi_i(\theta_k,\phi)|$ is the projection operator in the kth step if we divide the longitude to $\mathcal{N}$ steps. Physically, $W_{ij}(\phi)$ characterizes the probability of occupying either eigenstate at the south pole if the initial state is an arbitrary superposition of the eigenstate at the north pole after an adiabatic evolution along the longitude. $W_{ij}(\phi)$ is an orthogonal matrix and can be made real after an appropriate unitary transformation on $\hat{H}_{\text{eff}}$ (rotate $\hat{H}_{\text{eff}}$ to be real). Thus, $\xi(\phi) = W_{11}(\pi/2,\phi) + iW_{12}(\pi/2,\phi)$ defines a winding number $n_w = -\frac{i}{2\pi}\int_0^{2\pi} \xi^*(\phi)\partial_\phi\xi(\phi)$.

3D TOPOLOGICAL DEFECTS FOR EVEN NUMBER OF PARTICLES WITH REPULSIVE INTERACTION

For later convenience, we introduce R_A, R_B, ϕ_A, and ϕ_B, which are defined through $R_A e^{-I\phi_A} = R_x - iR_y$ and $R_B e^{-I\phi_B} = R_z n_x - iR_z n_y$. For $4m$ particles with strong repulsive interaction, the ground state is $|m,m,m,m\rangle$. No degeneracy is found.

For $4m+2$ particles with strong repulsive interaction, the ground state manifold has 6 states, $|m,m,m+1,m+1\rangle$, $|m,m+1,m,m+1\rangle$, $|m,m+1,m+1,m\rangle$, $|m+1,m,m,m+1\rangle$, $|m+1,m,m+1,m\rangle$, and $|m+1,m+1,m,m\rangle$. The Hamiltonian reads

$$\begin{pmatrix}
0 & 0 & -e^{i\phi_B}(m+1)R_B & -e^{i\phi_B}(m+1)R_B & 0 & 0 \\
0 & 0 & e^{i\phi_A}(m+1)R_A & -e^{i\phi_A}(m+1)R_A & 0 & 0 \\
-e^{-i\phi_B}(m+1)R_B & e^{-i\phi_A}(m+1)R_A & 2R_5 & 0 & -e^{i\phi_A}(m+1)R_A & -e^{i\phi_B}(m+1)R_B \\
-e^{-i\phi_B}(m+1)R_B & -e^{-i\phi_A}(m+1)R_A & 0 & -2R_5 & e^{i\phi_A}(m+1)R_A & -e^{i\phi_B}(m+1)R_B \\
0 & 0 & -e^{-i\phi_A}(m+1)R_A & e^{-i\phi_A}(m+1)R_A & 0 & 0 \\
0 & 0 & -e^{-i\phi_B}(m+1)R_B & -e^{-i\phi_B}(m+1)R_B & 0 & 0
\end{pmatrix} \tag{S33}$$

Two of the states, i.e. $(|0,0,1,1\rangle - e^{-2i\phi_B}|1,1,0,0\rangle)/\sqrt{2}$ and $(|0,1,0,1\rangle + e^{-2i\phi_A}|1,0,1,0\rangle)/\sqrt{2}$, have zero energy. Projecting out these two states, we write the effective Hamiltonian as a 4 by 4 matrix,

$$\begin{pmatrix}
2R_5 & \sqrt{2}e^{-i\phi_A}(m+1)R_A & -\sqrt{2}e^{-i\phi_B}(m+1)R_B & 0 \\
\sqrt{2}e^{i\phi_A}(m+1)R_A & 0 & 0 & -\sqrt{2}e^{i\phi_A}(m+1)R_A \\
-\sqrt{2}e^{i\phi_B}(m+1)R_B & 0 & 0 & -\sqrt{2}e^{i\phi_B}(m+1)R_B \\
0 & -\sqrt{2}e^{-i\phi_A}(m+1)R_A & -\sqrt{2}e^{-i\phi_B}(m+1)R_B & -2R_5
\end{pmatrix}. \tag{S34}$$

Rewriting the effective Hamiltonian using direct product of σ and τ matrices, we obtain

$$R_5(\tau_z+\sigma_z) + (R_1'\sigma_x + R_2'\sigma_y - R_3'\tau_x + R_4'\tau_y + \tau_z(R_3'\tau_x + R_4'\tau_y) + \tau_z(R_1'\tau_x - R_2'\tau_y)), \tag{S35}$$

where $R_1' = (m+1)(R_1-R_3)/\sqrt{2}$, $R_2' = (m+1)(R_2+R_4)/\sqrt{2}$ and $R_3' = (m+1)(R_1+R_3)/\sqrt{2}$, and $R_4' = (m+1)(R_2-R_4)/\sqrt{2}$. Solving the effective Hamiltonian, the eigen energies reads

$$\pm\sqrt{2}(m+1)\sqrt{\pm\sqrt{\left((R_A^2+R_B^2)+\frac{R_5^2}{(m+1)^2}\right)^2 - 4R_A^2R_B^2} + R_A^2 + R_B^2 + \frac{R_5^2}{(m+1)^2}}. \tag{S36}$$

Eigenenergies become degenerate in certain 3D continuous manifolds.

$\{\mathcal{M}_1\colon\ R_A = 0\}$ and $\{\mathcal{M}_1'\colon\ R_B = 0\}$, the second and the third states are degenerate, and the ground state (the fourth state) is unique.

$\{\mathcal{M}_2\colon\ R_5 = 0,\ R_A = R_B\}$, both the ground and excited states are doubly degenerate.

For M_1 and M_1', we find that the berry phase $\gamma = (0, 2\pi, 2\pi, 0)$ and $\zeta_1 = 0$ for the lowest two states. For M_2, we find that $\gamma = \pi$ for all eigenstates and $\zeta_1 = 0$ for the lowest two states.

We also rewrite the manifolds in the main text using R_A and R_B and find that the two type of 3D manifolds are switched with each other as the interaction strength changes from negative to positive. Furthermore, we have numerically verified that these degenerate manifolds extend to the weakly interacting regime.

LINKING NUMBER

In the 3D subspace with finite $|\vec{m}|$, e.g., $R_3 \neq 0$ and $R_4 = 0$, $\mathcal{M}_1$ and $\mathcal{M}_2$ are knotted nodal line and nodal ring. Thus, a linking number can be defined as follows,

$$L = \frac{1}{4\pi} \oint_{\mathcal{M}_1} \oint_{\mathcal{M}_2} \frac{\mathbf{r}_1 - \mathbf{r}_2}{|\mathbf{r}_1 - \mathbf{r}_2|^{\frac{3}{2}}} \cdot d\mathbf{r}_1 \times d\mathbf{r}_2. \tag{S37}$$

A straightforward calculation shows that L is always 1, which verifies that the two nodal surfaces are knotted in the subspace.

EXPERIMENTAL SCHEMES FOR EXPLORING FEW-BODY PHYSICS

There are a number of schemes to experimentally explore few-body physics related to the discussions in the main text, including optical superlattice, mesoscopic traps, optical tweezers, ion traps, and superconducting circuits.

As shown in Fig. S2(A), a 2D optical superlattice is formed by a short and long lattice with wavelengths $\lambda_L = 2\lambda_S$ [2, 3]. Such superlattice divides the system into many plaquettes. When the energy barrier between different plaquettes is large enough, plaquettes are isolated from each other. Each contains a few particles, and can be dressed and probed individually. In particular, high resolution in-situ images allow experimentalists to measure precisely the particle number per plaquette. Optical superlattices have allowed physicists to explore many interesting few-body phenomena in two sites or four sites.

To induce complex tunnelings among the four sites, either Raman dressing or shaking can be used. In the former approach, a field gradient can be applied in the diagonal direction to quench the bare tunnelings along both x and y directions [2, 3]. Then a pair of Raman laser induces a complex laser assisted tunneling. In fact, it is not necessary to individually control the phase of each tunneling. The key requirement is that the total effective magnetic flux per plaquette is π, i.e., a particle accumulates a π phase after finishing a closed loop composed of all four sites. Another approach is shaking the lattice [4, 5]. Theoretically, this is the same as the Raman dressed lattice. In practice, the advantage is that, no extra lasers are required. The onsite energies can be tuned by the two-photon detuning or the shaking frequency. An additional 1D optical lattice aligned in the diagonal direction can provide extra controls of the onsite energy. Using typical experimental parameters for Rb with scattering length $\approx$ 5nm and laser wavelength 767nm, we find that, interaction strength g in such lattice can reach 100Hz. For other atoms, Feschbach resonance could further enhance g. g is the characteristic energy scale of topological defects discussed here, for instance, the separation between different Yang monopoles in the parameter space and the energy gap in the effective models. With such g, topological defects can be easily resolved in current experiments.

One could also use four mesoscopic traps [6, 7], or optical tweezers to realize a four-site system that is equivalent to a single plaquette, as shown in Fig. S2(B). Two optical tweezers have been recently used to produce entangled pairs of atoms [8]. For instance, bringing four tweezers together and engineering the tunnelings between tweezers using external lasers, a single four-site model could be realized. Alternatively, one could stick to a single tweezer, and use four internal states of atoms. Theoretically, this would be equivalent to the NIST experiment. The advantage here is that, due to the strong confinement in an optical tweezer, the interactions could be much stronger. For instance, the typical confining potential of a single optical tweezer is 200kHz. For Rb with scattering length $a_s = 5nm$ and Cs with scattering length $a_s = 91nm$, such confinement corresponds to an interaction strength 1kHz and 24kHz, respectively. Thus, it will be much easier to explore interaction induced topological defects in optical tweezers.

Other quantum systems other than cold atoms can also be used to explore topological defects discussed in the main text. For instance, two nearby ion trap, each of which hosts a spin-1/2, can be used to realize the model in Eq.(7) of the main text, as shown in Fig. (S2.C). Here, (b, c) and (d, e) represent the magnetic field acting on the first and the second spin-1/2, which is denoted by $\vec{\sigma}$ and $\vec{\tau}$, respectively, in the $x - y$ plane. $a\sigma_z\tau_z$ is simply the Ising interaction. Similarly, two superconducting circuits may be used, as each circuit can be viewed as a spin-1/2 [9, 10]. Therefore, our theoretical results can also be generalized to superconducting circuits.

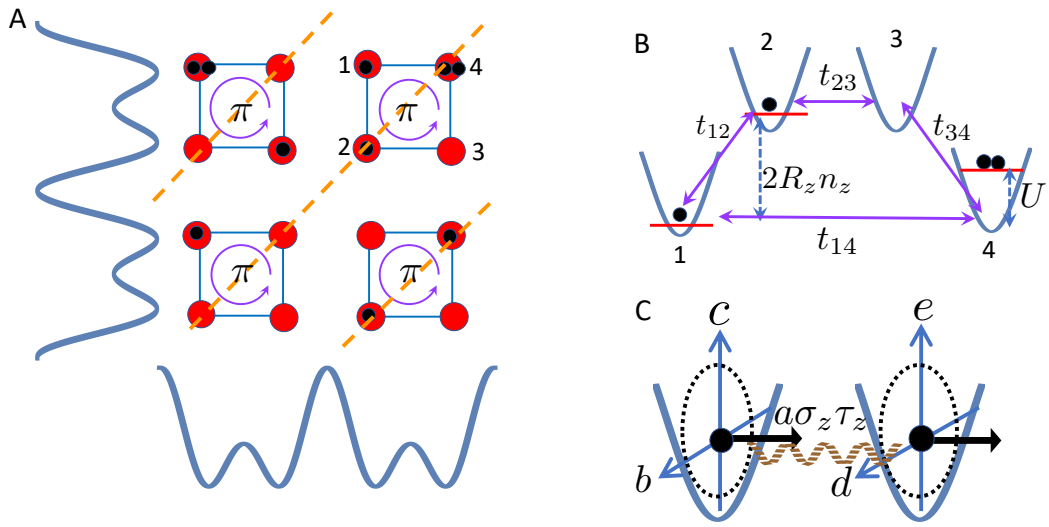

FIG. S2. (Color online) (A) Red spheres represent lattice sites of an optical superlattice and blue curves represent lattice potentials. Black spheres represent atoms. Orange dashed lines represent an additional lattice potential that shifts the onsite energies of two sites in each plaquette. (B) A schematic of the tunnelings and onsite energy in four mesoscopic traps, optical tweezers, or each plaquette of an optical superlattice. (C) Our results also apply to two ion traps, each of which hosts a spin-1/2 (black arrows).

GENERIC INTERACTION

A generic interaction $\sum_i g_i n_i^2 + \sum_{i\neq j} g_{ij} n_i n_j$ leads to corrections to the effective Hamiltonian discussed in the main text. As interactions transform to the onsite energy in the effective Hamiltonians constructed by four Fock states in Eq. (1) and Eq. (7) of the main text, nonuniform g_i and nonlocal $g_{i\neq j}$ (or equivalently, the inter-spin interaction in the spin model) only lead to corrections in the diagonal terms. Most generically, the corrections can be written as $\hat{H}'_{eff} = \sum_i \delta_i H'_i$, where

$$\begin{aligned} H'_1 &= \sum_{i=1}^{4} \hat{a}_i^\dagger \hat{a}_i, \\ H'_2 &= \hat{a}_1^\dagger \hat{a}_1 + \hat{a}_2^\dagger \hat{a}_2 - \hat{a}_3^\dagger \hat{a}_3 - \hat{a}_4^\dagger \hat{a}_4, \\ H'_3 &= \hat{a}_1^\dagger \hat{a}_1 - \hat{a}_2^\dagger \hat{a}_2 - \hat{a}_3^\dagger \hat{a}_3 + \hat{a}_4^\dagger \hat{a}_4, \\ H'_4 &= \hat{a}_1^\dagger \hat{a}_1 - \hat{a}_2^\dagger \hat{a}_2 + \hat{a}_3^\dagger \hat{a}_3 - \hat{a}_4^\dagger \hat{a}_4. \end{aligned} \tag{S38}$$

and δ_i corresponds to the strength of each type of perturbation.

δ_i depend on g_i and g_{ij}. For instance, the effective Hamiltonian near the origin of the parameter space for odd number of particles reads

$$\begin{pmatrix} -c_1 R_5 + \delta_1 + \delta_2 + \delta_3 + \delta_4 & -c_2 (R_1 - iR_2) & -c_2 (R_3 - iR_4) & 0 \\ -c_2 (R_1 - iR_2) & c_1 R_5 + \delta_1 + \delta_2 - \delta_3 - \delta_4 & 0 & -c_2 (R_3 - iR_4) \\ -c_2 (R_3 - iR_4) & 0 & c_1 R_5 + \delta_1 - \delta_2 - \delta_3 + \delta_4 & c_2 (R_1 - iR_2) \\ 0 & -c_2 (R_3 - iR_4) & c_2 (R_1 - iR_2) & -c_1 R_5 + \delta_1 - \delta_2 + \delta_3 - \delta_4 \end{pmatrix} \tag{S39}$$

where $c_1 = \tilde{\epsilon}_i/\epsilon_i$ and $c_2 = \tilde{t}_{ij}/t_{ij}$ [rewrite of Eq. (5) in the main text]. For three particles, $c_1 = -1$, $c_2 = 1$, and

$$\delta_1 = \frac{1}{4}\left(3g_1 + 3g_2 + 3g_3 + 3g_4 + 2g_{12} + 2g_{13} + 2g_{14} + 2g_{23} + 2g_{24} + 2g_{34}\right) \tag{S40}$$

$$\delta_2 = \frac{1}{4}\left(-g_1 - g_2 + g_3 + g_4 - 2g_{12} + 2g_{34}\right) \tag{S41}$$

$$\delta_3 = \frac{1}{4}\left(-g_1 + g_2 + g_3 - g_4 - 2g_{14} + 2g_{23}\right) \tag{S42}$$

$$\delta_4 = \frac{1}{4}\left(-g_1 + g_2 - g_3 + g_4 - 2g_{13} + 2g_{24}\right). \tag{S43}$$

For systems with equal intraspin interaction and no interspin interaction, i.e., $g_i = g$, and $g_{ij} = 0$, we obtain $\delta_1 = 3g$ and $\delta_2 = \delta_3 = \delta_4 = 0$. The Hamiltonian reduces to the unperturbed one.

For generic cases where $\delta_i \neq 0$, these four corrections H_i' can be classified into two categories.

Category 1: H_1' and H_3' respect time reversal symmetry of the effective Hamiltonian. H_1' only shifts the entire energy spectrum and does not change the topological defects. H_3' only shifts the position of the topological defects as a finite δ_3 simply changes the value of R_5 to R_5-δ_3. Therefore, the shape of topological defects and other results in the main text remain unchanged.

Category 2: H_2' and H_4' break the time reversal symmetry and new topological defects arise.

When only H_2' exists, i.e., $\delta_2 \neq 0, \delta_4 = 0$, the energy spectrum reads

$$E_{eff} = \pm\sqrt{\pm 2\sqrt{\delta_2^2\left(R_1^2 + R_2^2 + R_5^2\right)} + R_1^2 + R_2^2 + R_3^2 + R_4^2 + \delta_2^2 + R_5^2}. \tag{S44}$$

The two degenerate manifolds are obtained as follows.

1.$\mathcal{M}_1$, the first (third) and the second (fourth) states become degenerate when $R_5 = R_1 = R_2 = 0$.

2.$\mathcal{M}_2$, the second and the third states become degenerate when $R_5^2 + R_1^2 + R_2^2 = \delta_2^2$ and $R_3 = R_4 = 0$.

Apparently, $\mathcal{M}_1$ is an infinite 2D topological defect. In contrast, $\mathcal{M}_2$ becomes a finite 2D sphere, unlike $\mathcal{M}_2$ discussed in the main text, which extends to infinity. Thus, a finite δ_2 breaks the four-fold degeneracy at the original Yang monopole but retains the degeneracy between the second and the third states on a 2D sphere, $\mathcal{M}_2$.

Likewise, when only H_4' exists, i.e., $\delta_4 \neq 0, \delta_2 = 0$, we also obtain two degenerate manifolds,

1.$\mathcal{M}_1$, the first (third) and the second (fourth) state become degenerate when $R_5 = R_3 = R_4 = 0$.

2.$\mathcal{M}_2$, the second and the third states become degenerate when $R_5^2 + R_3^2 + R_4^2 = \delta_4^2$ and $R_1 = R_2 = 0$.

Again, $\mathcal{M}_1$ is an infinite 2D topological defect, and $\mathcal{M}_2$ is a finite 2D sphere.

When both H_2' and H_4' exit, i.e., $\delta_2 \neq 0$ and $\delta_4 \neq 0$, $\mathcal{M}_2$ can be written as,

$$\frac{R_5^2}{\delta_4^2} + \frac{R_3^2 + R_4^2}{(\delta_4^2 - \delta_2^2)} = 1, \quad |\delta_2| < |\delta_4| \tag{S45}$$

$$\frac{R_5^2}{\delta_2^2} + \frac{R_1^2 + R_2^2}{(\delta_2^2 - \delta_4^2)} = 1, \quad |\delta_2| > |\delta_4| \tag{S46}$$

For generic $\delta_2 \neq 0$ and $\delta_4 \neq 0$, Eqs. (S45) and (S46) describe an ellipsoid. It is clear that, when $\delta_2 = 0$ or $\delta_4 = 0$, Eqs. (S45) and (S46) reduce to the previous results. When $|\delta_2| = |\delta_4|$, $\mathcal{M}_2$ becomes a line segment connecting $(0, 0, 0, 0, -\delta_2)$ and $(0, 0, 0, 0, \delta_2)$, which signifies the transition from one ellipsoid in Eq.(S45) to the other in Eq.(S46).

In any case, if a 4D sphere encloses $\mathcal{M}_2$, C_2 remains unchanged. The reason is that, the second Chern number, as a topological invariant, is stable against small perturbations. Unless the perturbation is strong enough to close the energy gap between the second and the third energy eigenstates, C_2 remains the same. Thus, when the amplitudes of perturbations are much smaller than parameters of the single-particle Hamiltonian, for instance, the distance to the origin of the five-dimensional parameter space, R, results of C_2 in the main text remain unchanged.

We have also generalized the above results to the effective Hamiltonian for 3D continuous topological defects, i.e., the effective Hamiltonian in Eq.(7) of the main text. For two particles, if either δ_2 and δ_4 is zero, $\mathcal{M}_1$ is defined as $R_1 = R_2 = R_5 = 0$. If both δ_2 and δ_4 are finite, $\mathcal{M}_1$ does not exist. In contrast, $\mathcal{M}_2$ always exists. For finite δ_2 and δ_4, $\mathcal{M}_2$ is shifted to $R_5 = 0$ and $R_1^2 + R_2^2 + \delta_4^2 = R_3^2 + R_4^2 + \delta_2^2$. Thus, small nonuniform g_i and nonlocal interactions $g_{i\neq j}$ only lead to perturbative changes to the topological defects.

[1] T.-L. Ho and C. Li, "The Chern Numbers of Interaction-stretched Monopoles in Spinor Bose Condensates," arXiv:1704.03833.

[2] M. Aidelsburger, M. Atala, M. Lohse, J. T. Barreiro, B. Paredes, and I. Bloch, "Realization of the hofstadter hamiltonian with ultracold atoms in optical lattices," Phys. Rev. Lett. **111**, 185301 (2013).
[3] H. Miyake, G. A. Siviloglou, C. J. Kennedy, W. C. Burton, and W. Ketterle, "Realizing the Harper Hamiltonian with Laser-Assisted Tunneling in Optical Lattices," Phys. Rev. Lett. **111**, 185302 (2013).
[4] G. Jotzu, M. Messer, R. Desbuquois, M. Lebrat, T. Uehlinger, D. Greif, and T. Esslinger, "Experimental realization of the topological Haldane model with ultracold fermions," Nature (London) **515**, 237 (2014).
[5] C. V. Parker, L.-C. Ha, and C. Chin, "Direct observation of effective ferromagnetic domains of cold atoms in a shaken optical lattice," Nat. Phys. **9**, 769 (2013).
[6] A. N. Wenz, G. Zürn, S. Murmann, I. Brouzos, T. Lompe, and S. Jochim, "From Few to Many: Observing the Formation of a Fermi Sea One Atom at a Time," Science **342**, 457 (2013).
[7] G. Zürn, A. N. Wenz, S. Murmann, A. Bergschneider, T. Lompe, and S. Jochim, "Pairing in Few-Fermion Systems with Attractive Interactions," Phys. Rev. Lett. **111**, 175302 (2013).
[8] A. Kaufman, B. Lester, M. Foss-Feig, M. Wall, A. Rey, and C. Regal, "Entangling two transportable neutral atoms via local spin exchange," Nature (London) **527**, 208 (2015).
[9] P. Roushan, C. Neill, Y. Chen, M. Kolodrubetz, C. Quintana, N. Leung, M. Fang, R. Barends, B. Campbell, Z. Chen, *et al.*, "Observation of topological transitions in interacting quantum circuits," Nature (London) **515**, 241 (2014).
[10] M. D. Schroer, M. H. Kolodrubetz, W. F. Kindel, M. Sandberg, J. Gao, M. R. Vissers, D. P. Pappas, A. Polkovnikov, and K. W. Lehnert, "Measuring a Topological Transition in an Artificial Spin-1/2 System," Phys. Rev. Lett. **113**, 050402 (2014).